Solving fermion problems without solving the sign problem: Symmetry-breaking wave functions from similarity-transformed propagators for solving two-dimensional quantum dots

Siu A. Chin

Department of Physics and Astronomy, Texas A&M University, College Station, Texas 77843, USA

(Received 28 August 2019; accepted 17 March 2020; published 13 April 2020)

It is well known that the use of the primitive second-order propagator in path-integral Monte Carlo calculations of many-fermion systems leads to the sign problem. This work will show that by using the similarity-transformed Fokker-Planck propagator, it is possible to solve for the ground state of a large quantum dot, with up to 100 polarized electrons, without solving the sign problem. These similarity-transformed propagators naturally produce rotational symmetry-breaking ground-state wave functions previously used in the study of quantum dots and quantum Hall effects. However, instead of localizing the electrons at positions that *minimize* the potential energy, this derivation shows that they should be located at positions that *maximize* the bosonic ground-state wave function. Further improvements in the energy can be obtained by using these as initial wave functions in a ground-state path-integral Monte Carlo calculation with second- and fourth-order propagators.

DOI: 10.1103/PhysRevE.101.043304

I. INTRODUCTION

Two-dimensional, circular parabolically confined quantum dots are not only physical systems of great experimental interests [1] but are also mathematical models *par excellence* for the numerical study of the many-fermion problem. In contrast to real atoms, where the hydrogen atom's partition function is divergent [2], these "Hooke's atoms" [3] only have bound states, with convergent partition functions. This lack of additional complications allows us to focus attention solely on the effect of interaction and Fermi statistics. In this work we compute the ground-state energy of up to $N = 100$ spin-polarized electrons, the largest many-fermion quantum dot by the Monte Carlo method to date.

Quantum dots have been extensively studied by traditional methods of quantum many-body theory, such as Hartree-Fock (HF) [4], density functional theory (DFT) [5,6], configuration interaction (CI) [7], coupled-cluster (CC) [8,9], variational Monte Carlo (VMC) [10,11], diffusion Monte Carlo (DMC) [9,12,13], and path-integral Monte Carlo (PIMC) [14–19], with varying degrees of accuracy. However, with increasing number of electrons (say $N > 10$), basis-function-based methods, such as CI and CC, simply cannot keep up with the exponential growth of needed basis functions. For $N > 20$, even VMC and DMC have difficulties in constructing a good trial wave function involving many excited states. In principle, since PIMC does not require an initial trial wave function, it can be used to treat large quantum dots. However, PIMC can only extract the ground state at large imaginary time, and if many short-time antisymmetric propagators are used, then the resulting *sign-problem* will overwhelm the ground-state signal. One can side-step the sign problem in DMC and PIMC by invoking the fixed-node or the restricted-path approximation [19,20]. These approximations have worked surprising well and currently the ground-state energy of the largest spin-balanced quantum dot with $N = 60$ has been obtained using PIMC [19]. Here, we propose a new way of solving the fermion problem in large quantum dots without invoking any prior assumptions.

In Ref. [18], it was suggested that fourth-order propagators can be used in PIMC to reduce the number of antisymmetric propagators used and thereby reduce the severity of the sign problem. This is indeed a workable scheme for up to $N \approx 30$. However, beyond that, the sign problem remains severe at large imaginary time.

In this work, we overcome this fundamental problem by reducing the length of the imaginary time needed by doing PIMC on symmetry-breaking wave functions that are already very close to the ground state, that is, we apply a fermion ground-state path-integral Monte Carlo (FGSPIMC) method to quantum dots. While the bosonic GSPIMC method is well known [20,21], the fermionic version has only been tried previously in the context of shadow wave function [22].

To derive such a symmetry-breaking wave function, we first derive, from a new perspective, some basic results on similarity transformed propagators in Sec. II. In Sec. III, we show that the harmonic oscillator has the remarkable property that if its propagator is similarity-transformed by its ground-state wave function, the resulting Fokker-Planck propagator, even if only approximated to first order, yields the *exact* partition function of the harmonic oscillator. We show in Sec. IV that, when these Fokker-Planck propagators are antisymmetrized in the many-fermion case, they yielded the exact ground-state energies of noninteracting fermions in a harmonic oscillator. That is, a many-fermion problem has been solved *exactly* without knowing the exact propagator, the exact wave functions, or having to solve any sign problem. In Sec. V, we show that in the presence of pair-wise repulsive Coulomb interactions, the resulting Fokker-Planck propagator naturally produces spontaneous symmetry-breaking (SSB) wave functions previously used in the studies of quantum dots

and quantum Hall effects [4,23–25]. For quantum dots, we show that a variational version of these SSB wave functions can already yield energies to within 1% of the best ground-state energies. In Sec. VI, we show that this remaining 1% can be recovered by doing a FGSPIMC calculation using a fourth-order propagator. In Sec. VII, we summarize our conclusions and suggest future applications of this work.

II. SIMILARITY TRANSFORMED PROPAGATORS

For completeness, we will derive here some basic results in a new way. Let the imaginary-time propagator (or density matrix) of the Hamiltonian operator H be

$$G(\mathbf{x},\mathbf{x}';\tau)=\langle\mathbf{x}|e^{-\tau H}|\mathbf{x}'\rangle, \tag{1}$$

then corresponding partition function

$$Z(\tau)=\int d\mathbf{x}\, G(\mathbf{x},\mathbf{x};\tau) \tag{2}$$

is invariant under the similarity transformation

$$\begin{aligned} Z(\tau)&=\int d\mathbf{x}\langle\mathbf{x}|\phi e^{-\tau H}\phi^{-1}|\mathbf{x}\rangle\\ &=\int d\mathbf{x}\phi(\mathbf{x})G(\mathbf{x},\mathbf{x};\tau)\phi^{-1}(\mathbf{x})\\ &=\int d\mathbf{x}\, G(\mathbf{x},\mathbf{x};\tau), \end{aligned} \tag{3}$$

provided that $\phi(\mathbf{x})$ is nonvanishing and real at all $\mathbf{x}$,

$$\phi(\mathbf{x})\neq 0. \tag{4}$$

Therefore, $Z(\tau)$ can also be computed from the transformed propagator

$$\tilde{G}(\mathbf{x},\mathbf{x}';\tau)=\langle\mathbf{x}|e^{-\tau\tilde{H}}|\mathbf{x}'\rangle,$$

corresponding to the transformed Hamiltonian

$$\tilde{H}=\phi(\mathbf{x})H\phi^{-1}(\mathbf{x}). \tag{5}$$

Since $\phi(\mathbf{x})$ is nonvanishing everywhere, it can always be written as

$$\phi(\mathbf{x})=e^{-S(\mathbf{x})}, \tag{6}$$

which defines $S(\mathbf{x})$. We will call $S(\mathbf{x})$ the *action* of the wave function. For a single-particle Hamiltonian in D-dimension of the separable form,

$$H=-\tfrac{1}{2}\nabla^2+V(\mathbf{x})=K+V(\mathbf{x}),$$

the transformed Hamiltonian is

$$\tilde{H}=e^{-S(\mathbf{x})}Ke^{S(\mathbf{x})}+V(\mathbf{x}).$$

Since K is only a second-order derivative operator, the general operator identity

$$e^{C}Ke^{-C}=K+[C,K]+\tfrac{1}{2!}[C,[C,K]]+\tfrac{1}{3!}[C,[C,[C,K]]],\ \ldots \tag{7}$$

with $C=-S(x)$, terminates at the double commutator term:

$$e^{-S(\mathbf{x})}Ke^{S(\mathbf{x})}=K-[S,K]+\tfrac{1}{2}[S,[S,K]].$$

From the definition of $K=-\frac{1}{2}\nabla^2$, one has

$$[S,K]=\nabla S\cdot\nabla+\tfrac{1}{2}\nabla^2 S,\quad [S,[S,K]=-(\nabla S)^2$$

and therefore the transformed Hamiltonian is

$$\tilde{H}\psi=(K+D+E_L)\psi,$$

where D is the *drift* operator

$$D\psi=\nabla\cdot[\mathbf{v}(\mathbf{x})\psi],$$

with drift velocity $\mathbf{v}(\mathbf{x})=-\nabla S(\mathbf{x})$ and

$$E_L(\mathbf{x})=\frac{1}{2}\nabla^2 S-\frac{1}{2}(\nabla S)^2+V=\frac{H\phi(\mathbf{x})}{\phi(\mathbf{x})}$$

is the *local energy* function. The transformed imaginary time propagator is then

$$\tilde{G}(\mathbf{x},\mathbf{x}';\tau)=\langle\mathbf{x}|e^{-\tau(K+D+E_L)}|\mathbf{x}'\rangle. \tag{8}$$

The present derivation of this fundamental result on the basis of Eq. (7) is new, as far as the author can tell.

If E_L is a constant, then because of the nonvanishing condition Eq. (4), $\phi(\mathbf{x})$ must be the *bosonic* ground state $\psi_0(\mathbf{x})$ of H. In this case, Eq. (8) is the *Fokker-Planck* (FP) propagator whose long time stationary solution is the square of the ground-state wave function: $\phi^2(\mathbf{x})=\psi_0^2(\mathbf{x})$.

Even in cases where E_L is not a constant, the advantage of using the transformed propagator Eq. (8) is that low-order approximates of $\tilde{G}(\mathbf{x},\mathbf{x}';\tau)$ can be far more accurate than low-order approximates of $G(\mathbf{x},\mathbf{x}';\tau)$. For example, a first-order (in τ) approximation of Eq. (8) is

$$\tilde{G}_1(\mathbf{x},\mathbf{x}';\tau)=\langle\mathbf{x}|e^{-\tau K}e^{-\tau D}|\mathbf{x}'\rangle e^{-\tau E_L(\mathbf{x})}. \tag{9}$$

Since as shown in Ref. [26],

$$\begin{aligned} \langle\mathbf{x}|e^{-\tau K}|\mathbf{x}_1\rangle&=(2\pi\tau)^{-D/2}\exp\left[-\frac{1}{2\tau}(\mathbf{x}-\mathbf{x}_1)^2\right],\\ \langle\mathbf{x}_1|e^{-\tau D}|\mathbf{x}_0\rangle&=\delta[\mathbf{x}_1-\mathbf{x}(\tau)], \end{aligned}$$

where $\mathbf{x}(\tau)$ is the solution to the drift equation with initial position $\mathbf{x}_0$:

$$\frac{d\mathbf{x}}{d\tau}=\mathbf{v}(\mathbf{x})=-\nabla S(\mathbf{x}), \tag{10}$$

the resulting first-order propagator is

$$\begin{aligned} \tilde{G}_1(\mathbf{x},\mathbf{x}_0;\tau)&=\int d\mathbf{x}_1\langle\mathbf{x}|e^{-\tau K}|\mathbf{x}_1\rangle\langle\mathbf{x}_1|e^{-\tau D}|\mathbf{x}_0\rangle e^{-\tau E_L(\mathbf{x}_0)}\\ &=\frac{1}{(2\pi\tau)^{D/2}}\exp\left\{-\frac{1}{2\tau}[\mathbf{x}-\mathbf{x}(\tau)]^2\right\}e^{-\tau E_L(\mathbf{x}_0)}. \end{aligned} \tag{11}$$

This is to be compared with the first-order approximation of $G(\mathbf{x},\mathbf{x}_0;\tau)$:

$$\begin{aligned} G_1(\mathbf{x},\mathbf{x}_0;\tau)&=\int d\mathbf{x}_1\langle\mathbf{x}|e^{-\tau K}e^{-\tau V}|\mathbf{x}_0\rangle\\ &=\frac{1}{(2\pi\tau)^{D/2}}\exp\left[-\frac{1}{2\tau}(\mathbf{x}-\mathbf{x}_0)^2\right]e^{-\tau V(\mathbf{x}_0)}. \end{aligned} \tag{12}$$

The transformed propagator Eq. (11) replaces the bare potential $V(\mathbf{x})$, which can be highly singular, by $E_L(\mathbf{x})$, which can be a nonsingular and less fluctuating. It also replaces the aimless Gaussian random walk in $G_1(\mathbf{x}, \mathbf{x}_0; \tau)$ by Gaussian random walks along trajectories of the velocity field $\mathbf{v}(\mathbf{x}) = -\nabla S(\mathbf{x})$ produced by the trial wave function. This transformed propagator $\tilde{G}_1(\mathbf{x}, \mathbf{x}_0; \tau)$ is the basis for doing DMC [27,28] with importance-sampling and is the generalized Feynman-Kac path integral [29] when $\phi(\mathbf{x}) \neq \psi_0(\mathbf{x})$. In the next section, we will show that this FP propagator produces a remarkable result for the harmonic oscillator.

III. TRANSFORMED HARMONIC PROPAGATORS

Consider a D-dimensional harmonic Hamiltonian with energy in units of $\hbar\omega$ and length in units of $\sqrt{\hbar/m\omega}$,

$$H = -\tfrac{1}{2}\nabla^2 + \tfrac{1}{2}\mathbf{x}^2.$$

In this case, one can take $\phi(\mathbf{x}) = \psi_0(\mathbf{x})$, the exact ground-state wave function with action

$$S(\mathbf{x}) = \tfrac{1}{2}\mathbf{x}^2,$$

and a constant E_L,

$$E_L = \frac{1}{2}\nabla^2 S - \frac{1}{2}(\nabla S)^2 + \frac{1}{2}\mathbf{x}^2 = \frac{D}{2} \equiv E_0, \tag{13}$$

which is the exact ground-state energy.

The solution $\mathbf{x}(\tau)$ to the drift equation with initial position $\mathbf{x}_0$ is then simply

$$\frac{d\mathbf{x}}{d\tau} = \mathbf{v}(\mathbf{x}) = -\nabla S(\mathbf{x}) = -\mathbf{x} \;\rightarrow\; \mathbf{x}(\tau) = \mathbf{x}_0 e^{-\tau},$$

giving the first-order transformed propagator Eq. (11):

$$\tilde{G}_1(\mathbf{x}, \mathbf{x}_0; \tau) = \frac{1}{(2\pi\tau)^{D/2}} \exp\left[-\frac{(\mathbf{x} - \mathbf{x}_0 e^{-\tau})^2}{2\tau}\right] e^{-\tau E_L}. \tag{14}$$

This is to be compared to the exact FP propagator, corresponding to the Ornstein-Uhlenbeck [30] process:

$$\tilde{G}(\mathbf{x}, \mathbf{x}_0; \tau) = \frac{1}{[2\pi T(\tau)]^{D/2}} \exp\left[-\frac{(\mathbf{x} - \mathbf{x}_0 e^{-\tau})^2}{2T(\tau)}\right] e^{-\tau E_L}, \tag{15}$$

with

$$T(\tau) = \tfrac{1}{2}(1 - e^{-2\tau}). \tag{16}$$

In the limit of $\tau \to \infty$, this exact FP propagator correctly gives

$$\tilde{G}(\mathbf{x}, \mathbf{x}_0; \tau) \to \frac{1}{\pi^{D/2}} \exp[-\mathbf{x}^2] e^{-\tau E_0} = \psi_0^2(\mathbf{x}) e^{-\tau E_0}, \tag{17}$$

which is proportional to the *square* of the ground-state wave function. By contrast, the first-order transformed propagator $\tilde{G}_1(\mathbf{x}, \mathbf{x}_0; \tau) \to 0$ as $\tau \to \infty$ and bears no resemblance to any wave function. This seems to be a very poor approximation to the exact propagator. However, if one computes the partition function from this *single* transformed propagator,

$$\begin{aligned} Z &= \int d\mathbf{x} \tilde{G}_1(\mathbf{x}, \mathbf{x}; \tau) \\ &= \frac{1}{(2\pi\tau)^{D/2}} \int d\mathbf{x} \exp\left[-\frac{1}{2\tau}\mathbf{x}^2(1 - e^{-\tau})^2\right] e^{-\tau E_L} \\ &= \frac{[2\pi\tau(1 - e^{-\tau})^{-2}]^{D/2}}{(2\pi\tau)^{D/2}} e^{-\tau D/2} = \left(\frac{e^{-\frac{1}{2}\tau}}{1 - e^{-\tau}}\right)^D \\ &= [2\sinh(\tau/2)]^{-D}, \end{aligned} \tag{18}$$

then the result is *exactly* correct. That is, when the exact ground-state wave function, which knows nothing about τ, is used to derived the transformed propagator, the resulting single propagator calculation produces the correct $Z(\tau)$ at all τ, i.e., at all temperatures!

The only difference between the transformed first-order propagator Eq. (14) and the exact FP propagator Eq. (15) is that the variance of the Gaussian distribution is τ rather than $T(\tau)$. This single propagator calculation of $Z(\tau)$ is exact because the variance of the Gaussian distribution, after doing the integral, is canceled by the initial normalization constant and the integral is actually independent of the variance. This suggests that the solution to the drift equation, which is purely classical, is of unexpected importance for understanding quantum statistical dynamics, at least for the harmonic oscillator. In the next section, we will see how the drift term alone exactly solves the problem of many noninteracting fermions in a harmonic oscillator.

IV. NONINTERACTING FERMIONS IN A HARMONIC OSCILLATOR

In Eq. (17), one sees that the exact FP propagator yields the *square* of the ground-state wave function in the limit of $\tau \to \infty$ with

$$\mathbf{x}(\tau) \to 0 \quad \text{and} \quad T(\tau) \to \tfrac{1}{2}.$$

In the first-order transformed propagator Eq. (14), one also has $\mathbf{x}(\tau) \to 0$ as $\tau \to \infty$. What is left is then a Gaussian distribution with variance τ. If one now regards this variance τ as just a variational parameter and dissociates it from being the imaginary time needed to be set to infinity, then the choice of $\tau = 1$ would give the correct ground-state wave function (but not its square). This seems to be a rather contrived way of obtaining the ground-state wave function from the transformed propagator, but its utility is the following.

Consider N noninteracting particles in a D-dimensional harmonics oscillator. According to the above discussion, each particle's ground-state wave function would be (unnormalized)

$$\psi_0(\mathbf{x}_i) = \exp\left[-\frac{1}{2\tau}(\mathbf{x}_i - \mathbf{s}_i)^2\right],$$

with $\tau = 1$ and where $\mathbf{s}_i = \mathbf{x}(\tau \to \infty) \to 0$. However, for our purpose of antisymmetrization, we will only let each $\mathbf{s}_i$ approach close to zero but not exactly zero. For N spin-polarized fermions, as long as all $\mathbf{s}_i$ are distinct, one can construct the antisymmetric determinant wave function

$$\Psi(\mathbf{x}_1, \mathbf{x}_2 \ldots \mathbf{x}_N) = \det\left|\exp\left[-\tfrac{1}{2}(\mathbf{x}_i - \mathbf{s}_j)^2\right]\right|. \tag{19}$$

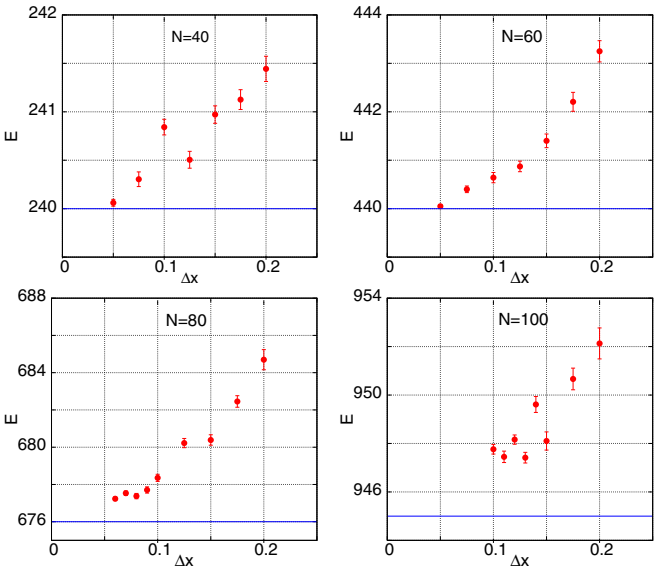

FIG. 1. The energy of N noninteracting, spin-polarized fermions in a 2D harmonic oscillator. For $N = 40, 60, 80, 100$, the exact energies, indicated by the horizontal blue line, are 240, 440, 676, and 945, respectively. The calculated lowest energies, at or near the smallest value of Δx, are 240.06(4), 440.05(3), 677.2(1), and 947.4(2). See text for details.

Remarkably, this simple wave function gives the *exact* energy of N noninteracting fermions in a harmonic oscillator so long as all $\mathbf{s}_i$ are close to zero but remain distinct from one another.

Recall that for a two-dimensional harmonic oscillator, the energy spectrum is given by $e(n_x, n_y) = n_x + n_y + 1$ (in units of $\hbar\omega$). There is one state with energy 1, two states with energy 2, three states with energy 3, and so on. The number of closed-shell states are $N = 1 + 2 + 3 + 4 + \cdots$ corresponding to energy $E = 1 + 2^2 + 3^2 + 4^2 + \cdots$, etc. For example, when $N = 10$, $E = 30$. Even when the shells are not closed for $N = 40, 60, 80, 100$, simple counting gives the exact energies as $E = 240, 440, 676, 945$. In Fig. 1, we show the energies computed from Eq. (19) in these four cases as $\{\mathbf{s}_j\}$ approaches zero.

These four calculations were done by generating N positions of $\mathbf{s}_i$ randomly near the origin with approximate separations of Δx. This is necessary to prevent $\mathbf{s}_i$ from overlapping, causing the determinant to vanish. The square of this wave function (no sign problem) is then sampled using the Metropolis *et al.* [31] algorithm. To compute the energy, it is necessary to compute the inverse of the matrix in Eq. (19). With decreasing Δx, particles are closer to each other and closer to the origin. For N up to 60, one sees that the calculation gives the correct energy up to statistical uncertainties. For $N > 60$, there is a systematic bias due to the limitation of double precision in Fortran. When N is large, the determinant is nearly vanishing and the routine for inverting the matrix is increasingly inaccurate. This prevents the calculation from being done at a Δx sufficiently small to give the correct result. This is shown in the case of $N = 80$ and $N = 100$. The use of multiprecision arithmetic would alleviate this purely numerical problem.

This wave function Eq. (19) for computing the noninteracting fermion energy is much simpler than antisymmetrizing excited states of the harmonic oscillator or using the exact harmonic oscillator propagator [18]. The reason why this wave function Eq. (19) is exact can be seen from formulas given in Refs. [23,24]. Here, we can give a simple example to illustrate the idea. For $N = 2$, the (unnormalized) antisymmetrized wave function is

$$\Psi(\mathbf{x}_1, \mathbf{x}_2) = e^{-[(\mathbf{x}_1-\mathbf{s}_1)^2+(\mathbf{x}_2-\mathbf{s}_2)^2]/2} - e^{-[(\mathbf{x}_1-\mathbf{s}_2)^2+(\mathbf{x}_2-\mathbf{s}_1)^2]/2}$$
$$= e^{-[(\mathbf{x}_1-\mathbf{s}_1)^2+(\mathbf{x}_2-\mathbf{s}_2)^2]/2}(1 - e^{-(\mathbf{s}_1-\mathbf{s}_2)\cdot(\mathbf{x}_1-\mathbf{x}_2)}). \tag{20}$$

In the limit of $\mathbf{s}_i \to 0$, the wave function to first order in $\mathbf{s}_1, \mathbf{s}_2$ is just

$$\Psi(\mathbf{x}_1, \mathbf{x}_2) = (\mathbf{s}_1 - \mathbf{s}_2) \cdot (\mathbf{x}_1 - \mathbf{x}_2) e^{-(\mathbf{x}_1^2+\mathbf{x}_2^2)/(2\tau)}, \tag{21}$$

which is proportional to the correct two-fermion wave function in the harmonic oscillator. Note that we must have $\mathbf{s}_1 \neq \mathbf{s}_2$, otherwise the wave function vanishes.

V. SPONTANEOUS SYMMETRY-BREAKING WAVE FUNCTIONS

From this point onward, we will only discuss the case of $D = 2$. For N fermions in a harmonic oscillator with Coulomb interactions, the Hamiltonian is given by [13]

$$H = -\frac{1}{2}\sum_{i=1}^{N} \nabla_i^2 + \frac{1}{2}\sum_{i=1}^{N} \mathbf{x}_i^2 + \sum_{i>j} \frac{\lambda}{x_{ij}}, \tag{22}$$

where $x_{ij} = |\mathbf{x}_i - \mathbf{x}_j|$. The similarity transformed propagator will yield the corresponding antisymmetric wave function

$$\Psi_D(\mathbf{x}_1, \mathbf{x}_2 \ldots \mathbf{x}_N) = \det \left| \exp\left[-\frac{1}{2\tau}(\mathbf{x}_i - \mathbf{s}_j)^2 \right] \right|. \tag{23}$$

Here, we will let the variance of the Gaussian distribution, τ, usually set to 1, be allowed to vary. As before, each $\mathbf{s}_i = \mathbf{x}_i(\tau \to \infty)$ is a *stationary* point of the trajectory $\mathbf{x}_i(\tau)$ obeying the drift equation

$$\frac{d\mathbf{x}_i}{d\tau} = -\nabla_i S(\mathbf{x}_1, \mathbf{x}_2 \ldots, \mathbf{x}_N), \tag{24}$$

with $S(\mathbf{x}_1, \mathbf{x}_2 \ldots, \mathbf{x}_N)$ being the action of the many-particle *bosonic* ground-state wave function:

$$\Psi_B(\mathbf{x}_1, \mathbf{x}_2 \ldots \mathbf{x}_N) = e^{-S(\mathbf{x}_1, \mathbf{x}_2 \ldots, \mathbf{x}_N)}.$$

Note that the set of stationary points satisfying $d\mathbf{x}_i/d\tau = 0$ correspond to $\nabla_i S(\{\mathbf{x}_i\}) = 0$, and they are positions that minimize $S(\{\mathbf{x}_i\})$ or that *maximize* the bosonic wave function. (The case of multiple local maxima will be discuss in later sections.) In the noninteracting case, we have seen in the previous section that antisymmetrizing the exact bosonic ground state produces the exact fermionic ground state.

With the added Coulomb interaction, the exact bosonic ground state is known only for two particles at coupling $\lambda = 1$ with

$$S(\mathbf{x}_1, \ldots \mathbf{x}_N) = \frac{1}{2}\sum_{i=1}^{2} \mathbf{x}_i^2 - \ln(1 + x_{12}), \tag{25}$$

and $E_0 = 3$. The drift equations from Eq. (24) are then

$$\frac{d\mathbf{x}_1}{d\tau} = -\mathbf{x}_1 + \frac{\hat{\mathbf{x}}_{12}}{1+x_{12}}, \quad \frac{d\mathbf{x}_2}{d\tau} = -\mathbf{x}_2 + \frac{\hat{\mathbf{x}}_{21}}{1+x_{12}},$$
$$\rightarrow \quad \frac{d\mathbf{x}_{\rm cm}}{d\tau} = -\mathbf{x}_{\rm cm}, \quad \text{and} \quad \frac{d\mathbf{x}_{12}}{d\tau} = -\mathbf{x}_{12} + \frac{2\hat{\mathbf{x}}_{12}}{1+x_{12}}.$$

Since the drift equations are just first-order differential equations, they can be solved easily by any numerical method to arrive at their stationary points. In the above case, the stationary points can be gotten simply by setting the τ-derivatives to zero:

$$\mathbf{s}_{\rm cm} = 0 \quad \text{and} \quad \mathbf{s}_{12} = \hat{\mathbf{x}}_{12}(0)$$
$$\rightarrow \quad \mathbf{s}_1 = \tfrac{1}{2}\hat{\mathbf{x}}_{12}(0), \quad \mathbf{s}_2 = -\tfrac{1}{2}\hat{\mathbf{x}}_{12}(0).$$

The two stationary points $\mathbf{s}_1$ and $\mathbf{s}_2$ are antipodal points on a circle of radius $R = 1/2$, oriented by the initial vector $\hat{\mathbf{x}}_{12}(0)$, which is entirely arbitrary. Thus, any two such antipodal points on the circle can be stationary points of the above drift equation. However, when a specific pair of points is inserted into the fermion wave function Eq. (23), the resulting wave function no longer respects the rotational symmetry of the original Hamiltonian. Thus, the transformed propagator naturally produces a *spontaneous symmetry-breaking wave function*, which has been extensively discussed in the literature [4,23,24], notably by Yannouleas and Landman [4,24,25]. In these earlier discussions, such a wave function was simply viewed as an ansatz, and it is therefore entirely reasonable to take $\{\mathbf{s}_i\}$ as particle positions that minimize the classical potential energy [11,23,24]. In this case, they would be antipodal points on a circle with $R = 2^{1/3}/2 = 0.62996$. Here, our derivation of this wave function from the transformed propagator showed that *these stationary points are to be determined by the maximum of the bosonic wave function*.

In Fig. 2 we compare the energies computed from the fermion wave function Eq. (23) using these two sets of stationary points with that from a five-fermion-propagator PIMC calculation using an optimized fourth-order propagator, as described in Ref. [18]. The top line gives the energy from using stationary points minimizing the potential energy. The bottom line gives the energy from using stationary points maximizing the bosonic wave function. This comparison clearly shows that one should use stationary points from the latter rather than from the former. Moreover, the fermion wave function Eq. (23) is optimal with $R = 1/2$; any other radius yields a higher energy.

The rotational symmetry of this wave function can be restored by integrating over the angle of $\hat{\mathbf{x}}_{12}(0)$, basically summing the wave function over all antipodal points on the circle. Such a *symmetry-restored* wave function [24,25] should have lower energy and *may* account for the difference of 0.0085(5) between this wave function's energy and that of PIMC. We will not bother correcting the symmetry-restoration energy here, since later on, such a symmetry-restoration is done automatically when we perform a ground-state path-integral Monte Carlo calculation in Sec. VI.

For three particles, the exact bosonic ground state is unknown. However, from the above discussion, by symmetry, the three stationary points must form an equilateral triangle with energy minimized by their distance from the origin. To

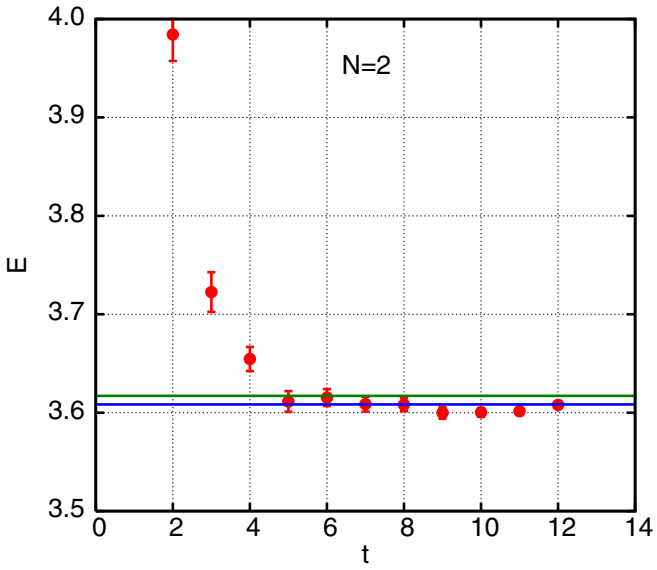

FIG. 2. Two-fermion energies at coupling $\lambda = 1$. Symbols are results from a five-fermion-propagator PIMC calculation using an optimized fourth-order fermion propagator [18] yielding a minimum energy of 3.600(4) at imaginary time $t = 10$. The top and the bottom line denote energy 3.6171(6) and 3.6085(5), respectively. See text for detail.

control the overall size of the triangle, we do not need the exact bosonic ground state; it is sufficient to use a trial ground state with action

$$S(\mathbf{x}_1, \mathbf{x}_2, \ldots \mathbf{x}_N) = \frac{1}{2}\sum_{i=1}^{N} \mathbf{x}_i^2 - \sum_{i>j} \frac{\lambda x_{ij}}{1+bx_{ij}}. \tag{26}$$

Here, the pairwise correlation function is well known to satisfy the 2D cusp condition with parameter b varying the strength of the correlation. (The cusp condition here is due to the bosonic ground state only and has nothing to do with whether the two particles are in a relative a spin-triplet or singlet state.) The resulting drift equation

$$\frac{d\mathbf{x}_i}{d\tau} = -\nabla_i S(\mathbf{x}_1, \mathbf{x}_2 \ldots, \mathbf{x}_N) = -\mathbf{x}_i + \sum_{j\neq i} \frac{\lambda \hat{\mathbf{x}}_{ij}}{(1+bx_{ij})^2} \tag{27}$$

can be solved numerically for any N to obtain the set of stationary points $\{\mathbf{s}_i\}$. With this correlator, as $\lambda \rightarrow 0$, $\mathbf{s}_i \rightarrow 0$, and the wave function Eq. (23) reduce to the exact wave function for N noninteracting fermions of the last section.

In Fig. 3, we compare the three-fermion energy at coupling $\lambda = 1$ using various form of the wave function Eq. (23) to that of a five-fermion-propagator PIMC calculation. The top most horizontal line is the energy resulting from using stationary points from minimizing the potential energy. The equilateral triangle is at $R = 0.83$. The next line down uses the correlation function of the exact two-fermion solution Eq. (25) giving $R = 0.75$. This shows that the correlation function which is exact for two-body may not be good enough for more than two bodies. The third line gives the energy using Eq. (26) at $b \approx 1$, but keeping $\tau = 1$, yielding $R \approx 0.50$. Finally, the

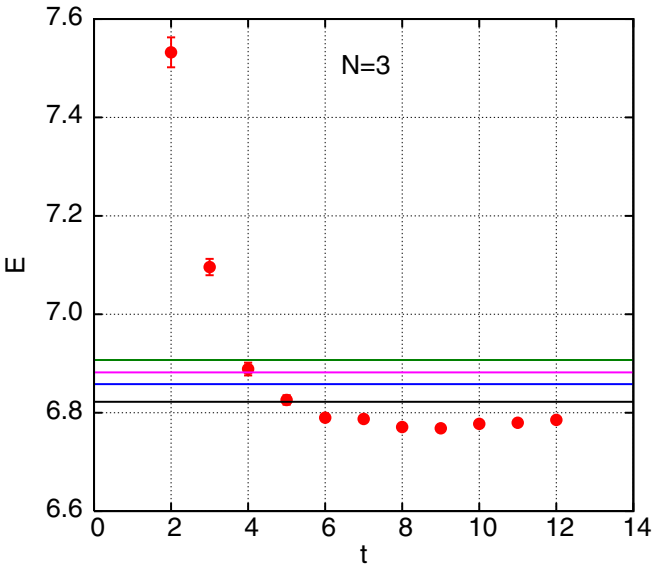

FIG. 3. Three-fermion energies at coupling $\lambda = 1$. Symbols show the five-fermion-propagator PIMC energy of 6.768(4) at $t = 9$. From the top down, the four horizontal lines are three-fermion energies of 6.907(1), 6.882(1), 6.858(1), 6.822(1), respectively, computed from various forms of the wave function Eq. (23). See text for detail.

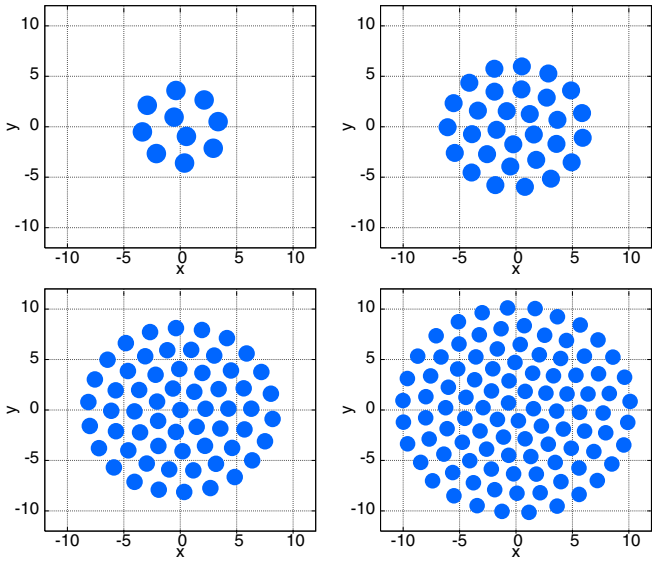

FIG. 4. Stationary points for the 10-, 30-, 60-, and 100-particle wave function at $\lambda = 8$ with each dot's radius set equal to $\sqrt{\tau}$.

lowest line corresponds to allowing τ to vary in addition to b. The minimum energy at $b = 1.7$, $\tau = 1.1$, which shrank R to ≈0.38 but broadened the Gaussian, is substantially better than varying b alone. The resulting energy is above the PIMC result by less than one percent.

As shown in Sec. IV, since our determinant wave function is exact in the noninteracting limit, it should be good at weak couplings. We therefore test the wave function here in the strong coupling limit of $\lambda = 8$. In Table I, the resulting energies from this two-parameter wave function for a 2D quantum dots with up $N = 100$ spin-polarized electrons are shown under the column SBWF, short for "symmetry-breaking wave function." The SBWF energies at this strong coupling are comparable to the two-fermion-propagator, fourth-order propagator results B2 from Ref. [18]. Since B2 is still a PIMC calculation, the energy needs to be extracted at an imaginary time of $\tau \approx 3$–4. At this value of τ, with more particles, the free-fermion determinant propagator is increasingly near zero, and its inversion needed for computing the Hamiltonian estimator limits the particle size to $N \approx 40$. Here, SBWF is like that of a free determinant propagator at only $\tau = 0.4$–0.8 and therefore can be used for up to $N = 100$ fermions, or more. Energies in other columns will be described in the next section.

With increasing number of fermions, Table I shows that b increases, weakening the interparticle repulsion, and τ decreases, making each Gaussian smaller. Both act to increase the particle density, but the quantum dot continues to expand in size with increasing number of fermions. This is shown in Fig. 4, where the stationary points of wave function Eq. (27) is plotted for 10, 30, 60, and 100 particles, with dot radius set equal to $\sqrt{\tau}$. (This gives a crude picture of the one-body density of the Bosonic wave function.) While the stationary points' concentric ringlike structure is very clear for 10 to 60 particles, and is similar to those determined by the classical potential energy [32], this ringlike structure is less clear for 100 particles. With increasing number of particles, there are many stationary configurations which are not strictly ringlike

TABLE I. Comparison of N *spin-polarized* 2D electron ground-state energies $E_0/\hbar\omega$ at coupling $\lambda = 8$.

N	τ	b	SBWF	B2[18]	GSPI2	GSPI4	PIMC[15]	CI[7]	DMC[12,13]
4	0.80	0.60	28.217(3)	28.266(5)	27.927(3)	27.818(5)	27.823(11)	27.828	
6	0.80	0.65	61.257(5)	61.403(7)	60.686(4)	60.475(6)	60.42(2)	60.80	60.3924(2)
8	0.70	0.67	104.21(1)	104.45(1)	103.425(8)	103.161(9)	103.26(5)		103.0464(4)
10	0.70	0.68	156.75(1)	156.77(1)	155.57(1)	155.23(1)			
20	0.65	0.70	537.56(2)	538.07(3)	534.71(5)	534.1(1)			
30	0.60	0.75	1091.60(4)	1091.7(1)	1086.5(1)	1085(1)			
40	0.60	0.74	1795.74(9)	1795.9(1)	1787.9(5)				
50	0.55	0.76	2636.73(6)		2627.0(3)				
60	0.50	0.78	3604.45(7)		3593(1)				
80	0.50	0.78	5893.2(3)						
100	0.45	0.80	8618.1(3)						

and only differ minutely in energy. Our algorithm for solving the drift Eq. (27) simply evolves a set of random initial positions for a long time, and therefore has no way of picking out only concentric ringlike configurations. It is also possible that at large N, rotational symmetry is broken entirely without any trace of discrete circular symmetry.

VI. FERMION GROUND-STATE PIMC

As we have shown in the last section, the determinant wave function Eq. (23) allows one to obtain excellent variational energies for up to 100 fermions (or spin-polarized electrons) in a 2D quantum dot. To lower the energy further, one can do a fermion ground-state path-integral Monte Carlo (FGSPIMC) calculation based on that trial function via

$$E_0 = \lim_{\tau\to\infty} \frac{\int d\mathbf{X}' d\mathbf{X}_1 d\mathbf{X} \Psi_D(\mathbf{X}') G(\mathbf{X}', \mathbf{X}_1; \tau) H G(\mathbf{X}_1, \mathbf{X}; \tau) \Psi_D(\mathbf{X})}{\int d\mathbf{X}' d\mathbf{X}_1 d\mathbf{X} \Psi_D(\mathbf{X}') G(\mathbf{X}', \mathbf{X}_1; \tau) G(\mathbf{X}_1, \mathbf{X}; \tau) \Psi_D(\mathbf{X})}, \tag{28}$$

where $G(\mathbf{X}', \mathbf{X}; \tau)$ can be either the commonly used second-order primitive propagator

$$G_2(\mathbf{X}', \mathbf{X}; \tau) = e^{-\frac{\tau}{2}V(\mathbf{X}')} \det \left| \exp\left[-\frac{(\mathbf{x}_i' - \mathbf{x}_j)^2}{2\tau} \right] \right| e^{-\frac{\tau}{2}V(\mathbf{X})}$$

or the fourth-order propagator corresponding to B2 of Ref. [18]. To preserve the upper bound property of the Hamiltonian estimator, it is necessary to evaluate H only at the middle of the integral. With antisymmetric propagators, evaluating H at any other position destroys this upper bound property. This greatly limited the choice of $G(\mathbf{X}', \mathbf{X}; \tau)$. If $G_2(\mathbf{X}', \mathbf{X}; \tau)$ is used, then Eq. (28) is a four-bead calculation, having essentially four antisymmetric free-propagators. If the fourth-order propagator $G_4(\mathbf{X}', \mathbf{X}; \tau)$ is used, each requiring two antisymmetric free-propagators, then Eq. (28) is a six-bead calculation. Both will then have sign problems, with the latter more severe. However, this GSPIMC calculation will still be better than doing a straightforward PIMC calculation. This is because for a PIMC calculation, the ground-state energy can only be extract at a relatively large imaginary time, such as $\tau \approx 8$, whereas evolving from $\Psi_D(\mathbf{X})$, one only needs $\tau \approx 3$ or less. This then greatly reduces the sign problem for determining the ground-state energy of a large quantum dot.

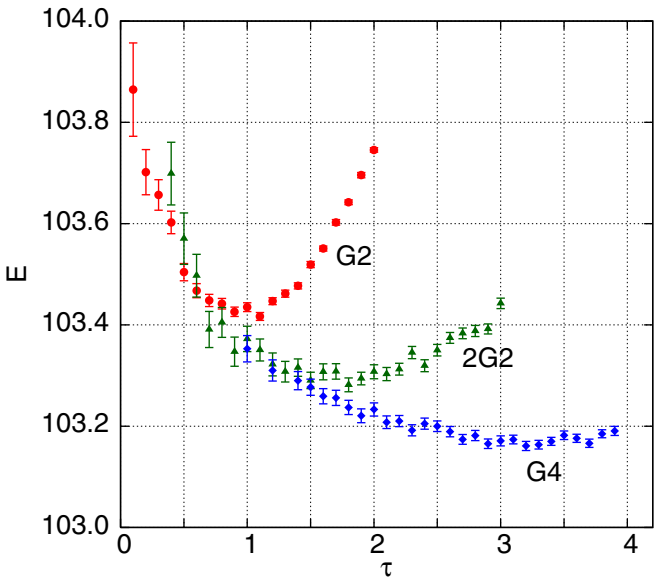

FIG. 5. Ground-state PIMC calculations for eight spin-polarized electrons in a 2D harmonic oscillator at coupling $\lambda = 8$ via Eq. (28). G_2 and G_4 are second and fourth-order imaginary time propagators respectively.

In Fig. 5, we show various GSPIMC calculations for the ground-state energy of eight spin-polarized electrons at $\lambda = 8$. Since G_4 uses two free-fermion propagators, we also computed the case with $2G2(\tau) = G_2(\tau/2)G_2(\tau/2)$, which is two second-order propagators at half the time step. The dramatic improvement in using G_4 is clearly visible. The flatness of the energy curve at large τ argues strongly that its energy is close to being exact. This is indeed the case, as shown in Table I, where the single G_2 and G_4 energies are shown under columns GSPI2 and GSPI4, respectively. While G_4 clearly refines the energy toward the exact, its improvement over that of G_2 is a mere ≈0.2% in the case of $N = 8$. By comparison, G_2 lowers the SBWF energy by ≈0.8%. Since G_4 is a six-bead calculation, due to the sign problem, it can only be used up to $N \approx 30$. G_2 remains effective for quantum dots twice as large, up to $N \approx 60$.

Since PIMC will diffuse away any asymmetry of the initial wave function and approach the exact symmetric ground state, doing a GSPIMC will automatically restore the broken symmetry of the initial state.

While the use of GSPIMC for solving bosonic systems is fairly common, its application to fermions, due to the sign problem, has not been as prevalent. The only other comparable method is the use of fermionic shadow wave function [22] (FSWF). However, the use of FGSPIMC here can take advantage of a fourth-order propagator, which is more difficult to implement in FSWF. Reference [22] has considered various choices for the free propagator, but if one views Eq. (28) as a form of fermion PIMC, then the natural choice is to use of the antisymmetric determinant propagator as done here.

VII. CONCLUSIONS AND FUTURE DIRECTIONS

In this work, we have shown that (1) similarity-transformed propagators, in the case of quantum dots, can naturally produce spontaneous symmetry-breaking (SSB) wave functions for solving many-fermion problems. This is a theoretical advance in that such a SSB wave function was previously regarded only as an *ad hoc* ansatz. (2) Our derivation show

that the particle positions of such a SSB wave function should be determined by maximizing the many-body bosonic wave function, rather than just minimizing the potential energy. (3) The use of such SSB wave function in solving the many-fermion problem via VMC is far simpler than using a determinant of excited states plus Jastrow correlators. (4) We have further demonstrated the usefulness of using higher-order propagators in the context of doing fermion GSPIMC.

A natural generalization of this work is to solve for case of spin-balanced quantum dots [19], with equal number of spin-up and spin-down electrons. However, the resulting SSB wave function now works less well due to *spin-frustration*. Take the example of $N = 6$ with $N_\uparrow = 3$ and $N_\downarrow = 3$. In each case of $N_\uparrow = 3$ or $N_\downarrow = 3$, the preferred configuration is an equilateral triangle. Therefore, for $N = 6$, the minimum energy configuration should be the interlacing of two equilateral triangles, forming a hexagon, with alternating spin at each vertex. However, for $N = 6$, the configuration which maximizes the bosonic wave function (or that of minimizing the potential energy) is a pentagon with a single particle at the center [32]. Therefore, one spin-up (or down) particle must be at the center. Such a wave function then frustrates the desired spin assignment and further breaks the spin-up/spin-down symmetry of the system. Moreover, for $N_\uparrow = N_\downarrow = N/2$, there are $N!/(2(N/2)!)$ distinct ways of assigning $N/2$ up spins and all are possible SSB wave functions. At this time, there is no known rule for determining which spin state will give the lowest energy. Alternatively, one can try to restore the spin-symmetry by summing over all states of distinct spin configurations. Such a multideterminant calculation would require an order of magnitude more effort and would be best done in a future publication.

For atomic calculations, there will not be SSB states. The calculation will most likely be similar to that of solving the noninteracting 2D harmonic oscillator, with $\{s_j\}$ approaching, but not equal to, zero. However, for nuclei calculations, since our method is exact for noninteracting fermions in a harmonic oscillator (which is essentially the shell-model), our method may be useful for calculating α-particle clustered nuclei such as C^{12}, O^{16}, Ne^{20}, etc., since α-particle clustering can be viewed as a SSB state.

ACKNOWLEDGMENT

Portions of this research were conducted with the advanced computing resources provided by Texas A&M High Performance Research Computing.

[1] S. M. Reimann and M. Manninen, Rev. Mod. Phys. **74**, 1283 (2002).
[2] S. M. Blinder, J. Math. Phys. **36**, 1208 (1995).
[3] N. R. Kestner and O. Sinanoglu, Phys. Rev. **128**, 2687 (1962).
[4] C. Yannouleas and U. Landman, Phys. Rev. Lett. **82**, 5325 (1999); **85**, 2220(E) (2000).
[5] M. Ferconi and G. Vignale, Phys. Rev. B **50**, 14722 (1994).
[6] K. Hirose and N. S. Wingreen, Phys. Rev. B **59**, 4604 (1999).
[7] M. Rontani and C. Cavazzoni, D. Bellucci, and G. Goldoni, J. Chem. Phys. **124**, 124102 (2006).
[8] E. Waltersson, C. J. Wesslen, and E. Lindroth, Phys. Rev. B **87**, 035112 (2013).
[9] M. Pedersen Lohne, G. Hagen, M. Hjorth-Jensen, S. Kvaal, and F. Pederiva, Phys. Rev. B **84**, 115302 (2011).
[10] A. Harju, S. Siljamaki, and R. M. Nieminen, Phys. Rev. B **65**, 075309 (2002).
[11] J. Kainz, S. A. Mikhailov, A. Wensauer, and U. Rössler, Phys. Rev. B **65**, 115305 (2002).
[12] F. Pederiva, C. J. Umrigar, and E. Lipparini, Phys. Rev. B **62**, 8120 (2000); Erratum: **68**, 089901 (2003).
[13] A. Ghosal, A. D. Güclü, C. J. Umrigar, D. Ullmo, and H. U. Baranger, Phys. Rev. B **76**, 085341 (2007)
[14] C. H. Mak, R. Egger, and H. Weber-Gottschick, Phys. Rev. Lett. **81**, 4533 (1998).
[15] R. Egger, W. Häusler, C. H. Mak, and H. Grabert, Phys. Rev. Lett. **82**, 3320 (1999); Erratum: **83**, 462 (1999).
[16] R. Egger, L. Mühlbacher, and C. H. Mak, Phys. Rev. E **61**, 5961 (2000).
[17] B. Reusch and R. Egger, Europhys. Lett. **64**, 84 (2003).
[18] Siu A. Chin, Phys. Rev. E **91**, 031301(R) (2015).
[19] I. Kylanpaa and E. Rasanen, Phys. Rev. B **96**, 205445 (2017).
[20] D. M. Ceperley, Rev. Mod. Phys. **67**, 279 (1995).
[21] A. Sarsa, K. E. Schmidt, and W. R. Magro, J. Chem. Phys. **113**, 1366 (2000).
[22] F. Calcavecchia, F. Pederiva, M. H. Kalos, and Thomas D. Kühne, Phys. Rev. E **90**, 053304 (2014)
[23] S. A. Mikhailov, Physica B **299**, 6 (2001).
[24] C. Yannouleas and U. Landman, Phys. Rev. B **66**, 115315 (2002).
[25] C. Yannouleas and U. Landman, Rep. Prog. Phys. **70**, 2067 (2007).
[26] Siu A. Chin, Phys. Rev. A **42**, 6991 (1990).
[27] J. W. Moskowitz, K. E. Schmidt, M. E. Lee, and M. H. Kalos, J. Chem. Phys. **77**, 349 (1982).
[28] P. J. Reynolds, D. M. Ceperley, B. J. Adler, and W. A. Lester, J. Chem. Phys. **77**, 5593 (1982).
[29] M. Caffarel and P. Claverie, J. Chem. Phys. **88**, 1088 (1988); **88**, 1100 (1988).
[30] G. E. Uhlenbeck and L. S. Ornstein, Phys. Rev. **36**, 823 (1930).
[31] N. Metropolis, A. W. Rosenbluth, M. N. Rosenbluth, A. H. Teller, and E. Teller, J. Chem. Phys. **21**, 1087 (1953).
[32] V. M. Bedanov and F. M. Peeters, Phys. Rev. B **49**, 2667 (1994).